Tellus (1995), 47A, 921–940
Printed in Belgium – all rights reserved

TELLUS
ISSN 0280–6495

Infrasonic signatures of a Polar Low in the Norwegian and Barents Sea on 23–27 March 1992

By JON BØRRE ØRBÆK*, *Department of Physics, University of Oslo, PO Box 1048 Blindern, N-0316 Oslo, Norway* and MAGNUS NAUSTVIK, *The Norwegian Meteorological Institute, PO Box 320 Blindern, N-0314 Oslo, Norway*

(Manuscript received 3 March 1993; in final form 11 April 1995)

ABSTRACT

This article presents an analysis of a Polar Low in the Norwegian and Barents Sea, 23–27 March 1992. The low is remote monitored from northern Norway and Svalbard by means of two Passive Broadband Infrasonic Sodars (PBIS's), estimating the directionality of the local acoustic field of atmospheric infrasound. The presented data show that the polar low apparently generates strong infrasound, and it is believed that some part of the measured pressure perturbations are generated by the intense turbulent regions of the low, as part of the aerodynamic spectrum. Due to the very low attenuation of infrasound in the atmosphere, the sound propagates to distant recording stations more than 1000 km away, by successive reflections between the upper atmosphere and the sea surface. Because of the small number of synoptic stations in the area, data inputs to the numerical circulation models are few, and because the phenomena in study are mesoscale, down to one tenth the size of a frontal cyclone, conventional meteorological data may not resolve the features of interest. The infrasonic direction-of-arrival (DOA)-spectra produced by the PBIS passive acoustic remote sensing technique utilized in this work, is shown to give new information to the analysis of the weather situation. While the satellite images normally are ambiguous with respect to the dynamics and thermodynamic state of the visible cloud-clusters, the infrasonic DOA-spectra may provide valuable dynamic information of the distant polar low in near real time. It is suggested that the major part of the infrasonic signatures detected by the PBIS's come from the active regions of turbulent convection. By picking out the directions of these active intensification regions, the DOA-spectra may, as is shown in this article, indicate that several local disturbances took part in the complex polar low development.

1. Introduction

The Norwegian, Greenland and Barents Sea region is a place of intense weather activity during the winter season. Frontal cyclones may be forced up from the Atlantic as a wave on the polar front, creating a maximum frequency of thunderstorms along the Norwegian coast at this time. Far north of the polar front, small mesoscale low pressures frequently develop as cold air from the ice-covered arctic streams southwards out over the relatively warm open waters. Because of the scattered weather observations in the area, these "polar lows", of a size only a tenth of a frontal cyclone, have traditionally been very difficult to detect and forecast. Many tragic accidents along our coast have been caused by these intense lows, often appearing without any prewarning. The wind may increase from calm to gale within 2 h when a polar low approaches, and the intense precipitation causes the visibility to be very low. In order to develop methods to improve the operational forecasting of these small disturbances, the "Polar Lows Project" (PLP) was started in January 1983. In addition to numerous case studies and direct measurements, better (fine mesh) numerical modeling of the lower atmosphere, as well as infrared imaging by polar orbiting satellites, have led to an increased general knowledge of the

* Corresponding author.

structure and generation mechanisms of the phenomena (PLP, 1986). However, in order to further improve the prediction situation, denser and more frequent data outputs from the conventional observing systems are necessary.

The development of these arctic "instability" lows may be caused by the release of baroclinic instability and/or CISK, Conditional Instability of Second Kind. Baroclinic instabilities here refer to a wave disturbance on a secondary arctic front or the baroclinic zones normally present along the ice-edge separating cold and warm air masses, while the CISK mechanism emphasizes the instability of the air-mass in question and postulates a simple feedback between the convective heating rate and the larger scale disturbances (cyclonic windfield) (Økland, 1987; Rasmussen, 1985). Whereas the baroclinic disturbance may provide the initial vorticity of the lows, CISK is often believed to be responsible for the rapid intensification seen. The satellite images often reveal high and cold cloud tops over the central part of the lows, and a large area of the surrounding ocean is covered with warmer (boundary layer) stratocumulus. The intense precipitation following the polar lows (Rabbe, 1975), give further evidence that convection of a rather deep nature is present. Pilot observations of a polar low (Rabbe, 1987), showed a dense, continuous cloud system all the way through the troposphere, and the slope of the cloud system was observed to be much steeper than compared to a normal synoptic scale warm front, indicating that the vertical velocities also should be higher. Økland (1989) then strongly argues that heating by organized, deep cumulunimbus convection is an important feature of the polar lows. Regarding the efficiency of the CISK mechanism, the precipitation and thus the net release of latent heat will be greater for deep convection than for the more shallow precipitation mechanisms.

It is now well known that severe convective storms may radiate a considerable amount of acoustic power into the atmosphere (Georges, 1973). The major part of the power is found in the mHz range, but storm related infrasound at higher frequencies (2 Hz) has also been recorded (Liszka, 1977). Strong turbulence is believed to be the most likely source for this aerodynamic sound, being a common process of wave emission in stellar and planetary atmospheres. The generation of acoustical waves by isotropic turbulence in an homogeneous atmosphere was first theoretically discussed by Lighthill (1952). While the energy source by Lighthill was taken from the mean fluid flow, Stein (1967) extended the theories to isothermal, stratified atmospheres and convection. Recently, Goldreich and Kumar (1990) have discussed the acoustic generation power of turbulence in a more realistic model atmosphere. They relate the total energy flux F_a carried by the acoustic waves to the convective energy flux F_c by the efficiency relation (following Lighthill, 1952):

$$F_a \propto M_t^{15/2} F_c.$$

Here, M_t is the turbulent Mach number, $M_t = v_t/c$, the ratio between the turbulent fluctuations and the speed of sound. The turbulent fluctuations are subsonic, i.e., $M_t \ll 1$. This source of aerodynamic sound production is therefore usually a very weak one. However, the relation for this aerodynamic model shows that the generation of sound is concentrated to the top of the convective layer, because the Mach number peaks there. Cold and high cloud tops should thus generate the major part of the sound.

Some correlation between cloud top height and the intensity of infrasound emissions were also found experimentally (Bowman and Bedard, 1971). Also, the turbulence intensity is closely related to the static stability of the atmosphere and its thermal stratification. Thus, it is reasonable to believe that the polar "instability" lows, due to the intense convective currents caused by the low stability of the convective central layer, may be strong acoustic generators. And because organized convection of a rather deep nature should be responsible for the rapid intensification as proposed by CISK, as well as the apparently strong threshold effect indicated by the high power of the conversion efficiency $M_t^{15/2}$, the emission intensity should be expected to increase sharply as the turbulent cloud-tops nears the tropopause.

Now, the infrasonic part of these emissions will, by the relatively weak attenuation of low frequency acoustical waves in the atmosphere (being proportional to the square of the wave frequency), propagate through the atmosphere by successive reflections between the natural temperature inversions of the upper atmosphere (at 30–50 km and 100–150 km height) and the sea surface, and may thus be detected at distant recording stations more than 1000 km away.

This article presents infrasound measurements of a polar low in the Norwegian and Barents Sea observed in the period 23–27 March 1992. The recordings are made by two Passive Broadband Infrasonic Sodars (PBIS's) (Ørbæk, 1992), situated in Skibotn (69.4° N, 20.3° E), northern Norway and at Hornsund (77.0° N, 15.6° E), Svalbard. Each system, consisting of a three-microphone array, estimates the directionality of the local atmospheric noise at a frequency range of about 0.2–13 Hz. It is believed that the major part of this noise background is produced by the turbulent processes in regions of intense weather activity, and the PBIS's can therefore be used for remote sensing of these areas. The polar low in study develops outside the coast of northern Norway, and it is monitored during its more intensive lifetime on its way up towards Svalbard and back again. Detailed analysis of the case reveals that the developing system rather consists of a series of smaller disturbances, interacting to produce this "long-lived" polar low. The article suggests that the PBIS information gives valuable information to the analysis of the weather situation, pointing out the directions of the active, convective clouds, or being able to detect new intensification of such cloud-clusters.

2. Case description

The polar low studied here developed in a typical situation of strong westerly upper air current located over the Greenland- and Norwegian-Sea. Between the Greenland high and a relatively stationary low at Novaya Semlya, cold arctic air was advected southwards in the Barents- and Norwegian-Sea area. A frontal low was centred over southern Norway, with its respective warmfront proceeding eastwards over Finland and the coldfront south of Britain, i.e., more than 1000 km away from the new, local development. The cold air outbreak appears in the satellite images as long and regular cloudstreets over the open sea to the west of Spitsbergen (see Fig. 3). Also visible in the figures (Fig. 3a) is a shear zone along the west coast of Svalbard and southwards towards Bear Island (74.5° N, 19.2° E). The Ice and Sea-Surface-Temperature (SST) map of Fig. 1, shows that shallow baroclinic zones with large

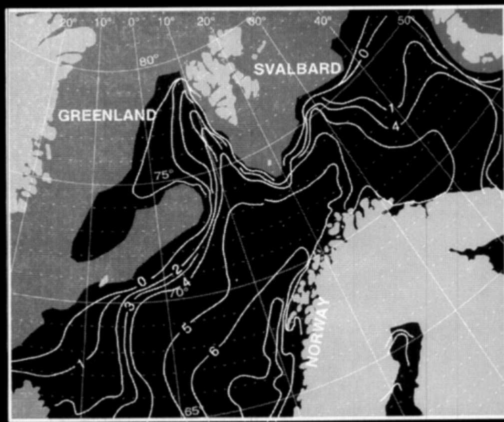

Fig. 1. Sea surface temperature and ice map 23 March 1992.

horizontal temperature gradients can exist in this area, as well as along the eastern coast of Greenland and in the Barents Sea northeast of northern Norway. As the cold arctic boundary layer air streams southwards from the ice towards the open sea, it is regularly perturbed by small vortices generated along these zones, as well as being gradually supplied by large fluxes of sensible and latent heat from the relatively warm sea surface below. And often, if the static stability of the whole air-mass is low enough, the vortices may develop into strong polar lows. We shall see that the development described in this case study, actually consists of three disturbances having their origin along these three different and widely separated zones. Fig. 2 shows a plot of the polar low trajectory during the whole development in the period

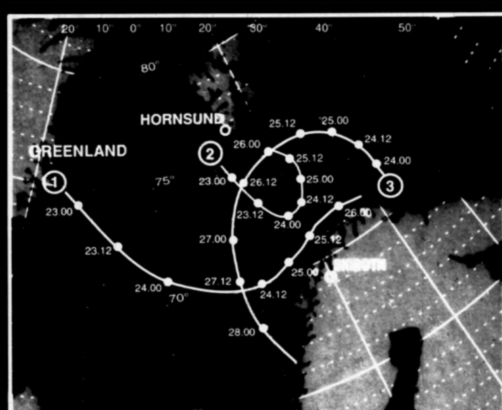

Fig. 2. Polar low trajectory 23–27 March 1992.

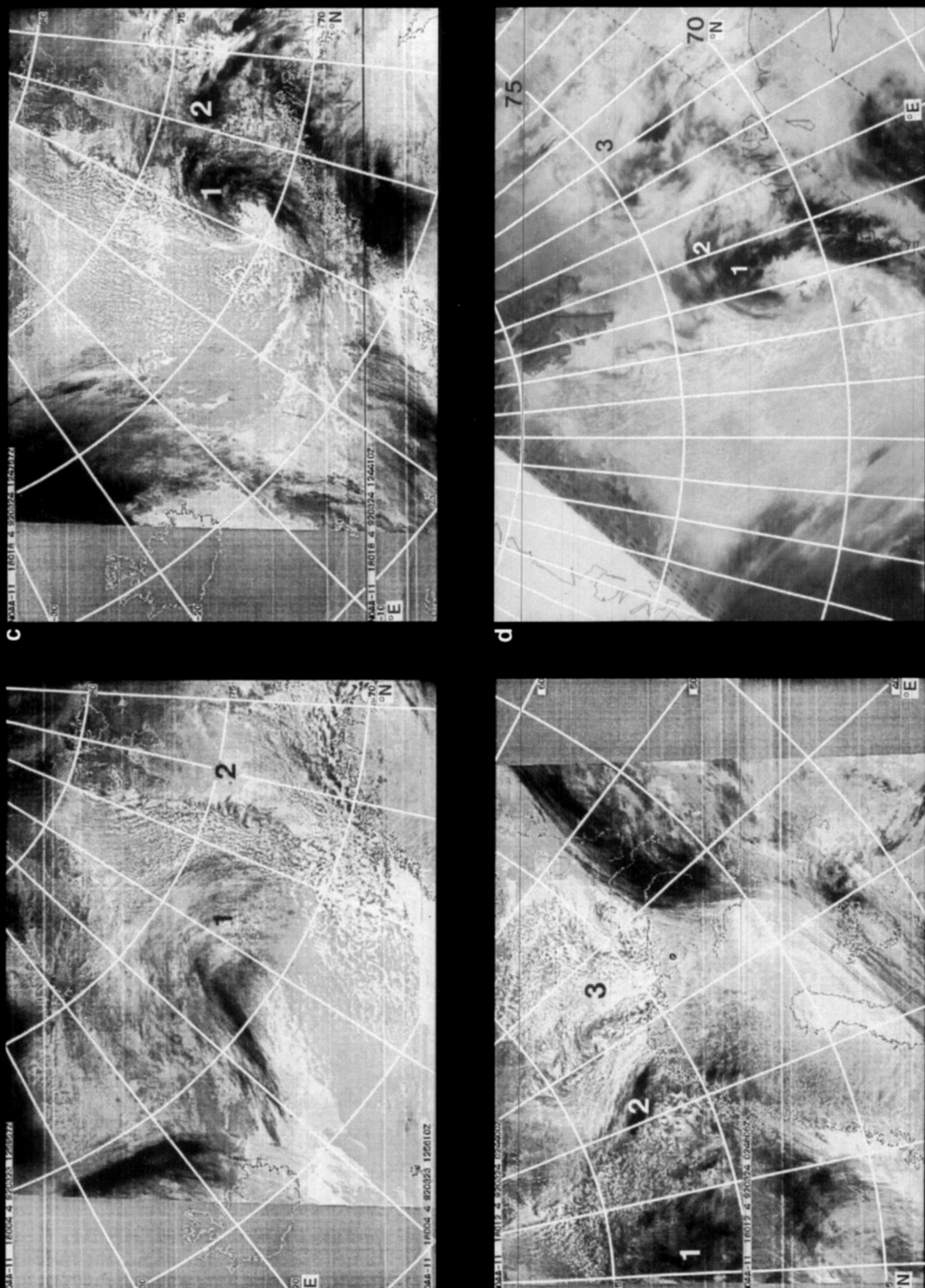

Fig. 3. NOAA-11 satellite images at 12.59 UTC 23 March (a), 02.44 UTC 24 March (b), 12.47 UTC 24 March (c), 16.16 UTC 24 March (d), 1992, Spacetec, Tromsø.

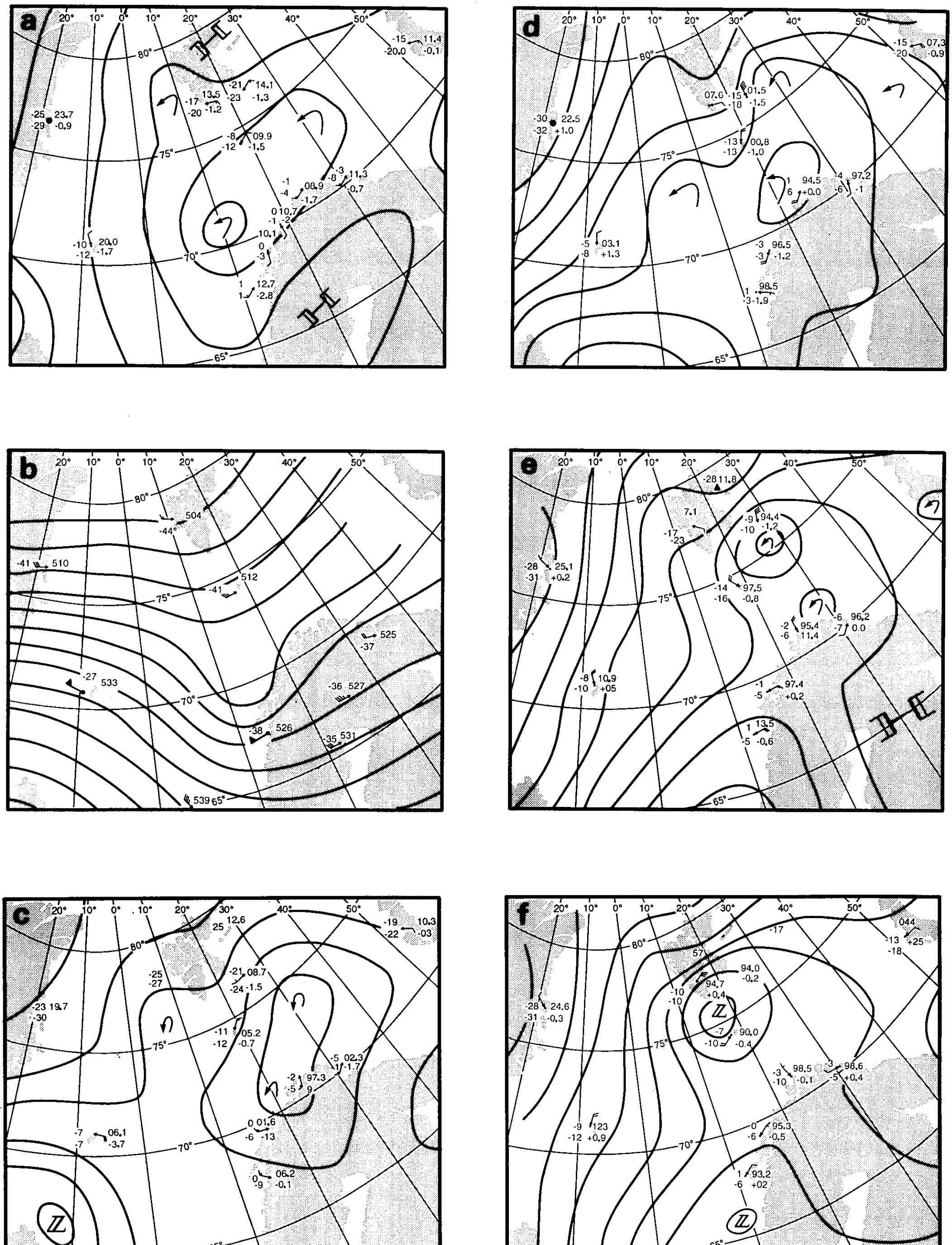

Fig. 4. Surface map (a), 500 hPa map (b), at 12 UTC 24 March 1992, Surface maps at 00 UTC (c), 12 UTC (d), 25 March 1992, Surface maps at 00 UTC (e), 12 UTC (f), 26 March 1992.

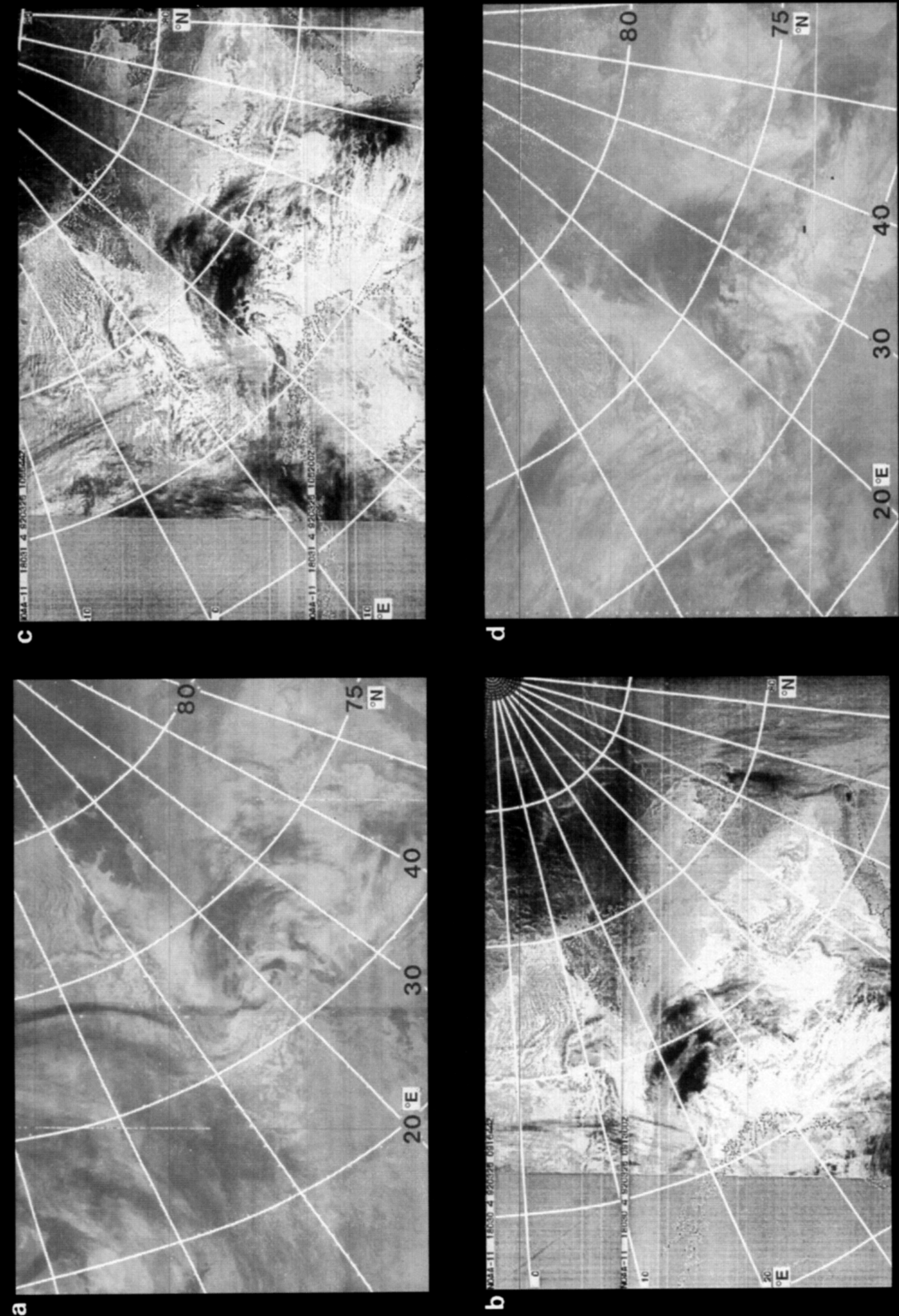

Fig. 5. Satellite images: NOAA-11 (DNMI) at 04.26 UTC (a), NOAA-11 (Spacetec) at 09.16 UTC (b), NOAA-11 (Spacetec) at 10.55 UTC (c), NOAA-12 (DNMI) at 15.54 UTC (d), 25 March 1992, NOAA-11 (Spacetec) at 02.20 UTC (e), NOAA-11 (Spacetec) at 12.24 UTC (f), 26 March 1992, NOAA-11 (DNMI) at 02.20 UTC (g), NOAA-12 (DNMI) at 16.15 UTC (h), 27 March 1992.

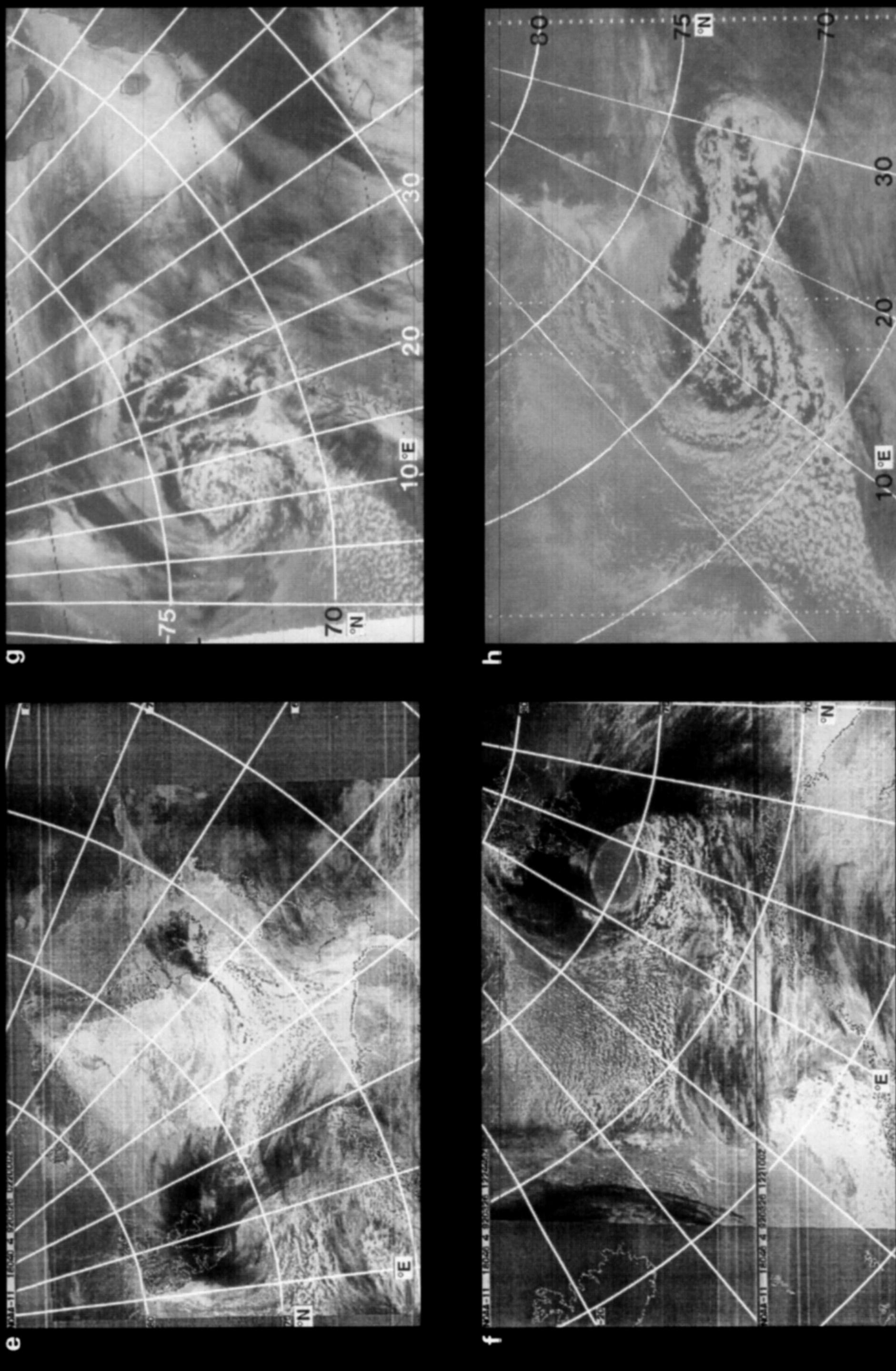

Fig. 5 (cont'd).

23–27 March. All three disturbances, marked 1, 2 and 3, are a consequence of the same cold air outbreak. As they move close together north of northern Norway during the 24th, the weather situation may be regarded as one larger system, built up as a cluster of smaller disturbances, which mutual interactions may explain the complex paths.

The first disturbance starts north of Jan Mayen (70.9° N, 8.7° W) on the 23rd, where a westerly airflow with relatively low stability and strong vorticity in the upper layers, migrates out from Greenland. The air-mass was very stable with very low 500 hPa temperatures (near −40°C) and surface temperatures of about −20°C. As the cold air-mass streams out over the relatively warm waters, a mesoscale disturbance develops, following the upper air currents towards the coast of northern Norway. This is seen in Fig. 3a as a cloud-cluster (marked 1) of a somewhat diffuse character surrounded by the low level stratocumulus cover.

The disturbance is slightly visible on the model surface maps as a trough line, but no ground observations are available from the time the system leaves the Jan Mayen area, until it reaches the Norwegian coast. However, as the actual cold air streams southeastwards, the boundary layer is rapidly destabilized by the heating from below, gradually eroding away the low level stable inversion layer. Regions of conditionally unstable air are formed, caused by the strong surface fluxes of heat and moisture. The satellite image of Fig. 3b shows that as the trough approaches the coast of northern Norway in the morning of the 24th, the boundary layer air is well mixed, and a large part of the Norwegian Sea is covered by diffuse convective clouds of localized intensity. It is interesting to note, that this development rapidly accelerated as the air-mass reached the area east of Jan Mayen where the SST shows a steep gradient (cf. Fig. 1). During the next 10 h, a centre of rotation develops, and the cloud cluster concentrates into a strong polar low vortex with its centre at approximately 71° N, 12° E at 12.47 UTC (Fig. 3c). The low is not accompanied by any strong wind increase at the coast stations, as seen on the surface map of Fig. 4a. It is also interesting that the development coincides with the time upper level positive vorticity is advected into the area, as seen from the cyclonic curvature of the 500 hPa contour lines of Fig. 4b.

The convective cloudband now stretches down to Lofoten and the coast of Nordland, and the radiosonde ascents from the area show that the air mass in question have been heated considerably in the lower layers and converted from stable to conditionally unstable conditions. Vigorous convection, extending at least up to 500 hPa height, is therefore expected near the centre of the low. The polar low probably becomes strongest at about 14 UTC (between Figs. 3c, d). Strong winds are expected to be seen on the southwestern side of the centre, but the winds are still weak at all synoptic stations along the coast. However, the pressure fall at the coast stations is significant, and the low can be followed moving slowly northeastwards along the coast during the day. Now, the further development is more complex and seems to be built up of several interacting disturbances. The small vortex marked 2 on Fig. 3a, is advected southwestwards preceding the first polar low, and appears as a new, growing cluster of convective clouds north of northern Norway in Fig. 3b. A third, shallow vortex is seen even further east. While the first polar low is most powerful, the second disturbance is also intensifying, moving slightly towards the north (Fig. 3c). Fig. 3d shows the situation at 16.16 UTC (24th). The clouds from polar low 1 and disturbance 2 now seem to merge to form a more complex cluster of clouds. By the same time, the eastern system (disturbance 3) has also intensified.

Figs. 4c, d shows the surface maps at 00 UTC and 12 UTC on the 25th. The first low is placed outside the coast of Finmark, with the other vortices located east and northeast of Bear Island. A disturbance is certainly located east of Hopen where a wind increase from 5–40 kn were recorded during this period. However, the development during the 25th is somewhat ambiguous, as is often seen in a polar low event like this. During its lifetime, it may consist of at least 2 interacting vortices. When the first one has released its energy, a new cell develops and takes another direction of movement. For later reference, several satellite images are used to describe the further development (Fig. 5a–f). Fig. 5a shows a cluster with several bright, convective clouds in the morning of the 25th at 04.26 UTC. The first polar low is now difficult to see on the satellite images, but it can still be seen on the surface maps, following the trajectory marked out in Fig. 2. At 9.16 UTC

(Fig. 5b) the second and third disturbances seem to have moved closer on their way northwards, and a complex cluster of 4–5 separate, intense convective areas is seen. The cloud-cluster further intensifies northwards, passing on the eastern side of Bear Island (Fig. 5c). At 12 UTC the disturbance reaches the Hopen station, reporting windspeed at 40 kn. Towards evening at 15.15 UTC, the clouds cover a large region southeast of Svalbard (Fig. 5d), and by midnight 25–26 March the low centre turns westward north of Bear Island, the clouds blow over the southern tip of Svalbard (Fig. 5e), and the windfield at the Hornsund station increases sharply from 6–44 Kn in 3 h. The surface maps now place the low centre at a position northeast of Bear Island (Fig. 4e). The low now moves westward north of Bear Island, and around midday (Fig. 5f), a clear rotation centre is seen, with extensive clouds covering large areas on the eastern and western side of Svalbard. This second polar low has now probably reached its maximum intensity, with the central pressure below 990 hPa (Fig. 4f).

The radiosonde profiles from Bear Island at 00 UTC on the 26th and 27th are included in Fig. 6. The initial stable and dry air (thick line) is replaced by an air column that approximately follows the wet adiabate as the low passes the station (thin line). This remarkable change of the air-mass over Bear Island is likely to be caused by the advection from the southeast of the cold, unstable layer between 700 and 500 hPa, and supply of cold boundary layer air from northeast, destabilized by the heating from below.

During the 26th, the low moves slowly southwards again, passing on the western side of Bear Island. In the morning of the 27th, the low is seen southwest of Bear Island (Fig. 5g). The extensive clouds have disappeared, but rainbands are still seen distributed around the rotation centre, in an area of approximately 400 km in diameter. The centre moves further south, it splits, and a front zone develops east-west on the northern side, where active, convective clouds once again are concentrated, as shown by the satellite image of Fig. 5h. The low finally made landfall at Lofoten on the 28th.

It should be stressed that the northward intensification of the complex cluster of clouds during the 25th is rather ambiguous. The satellite images do not give much information about the wind

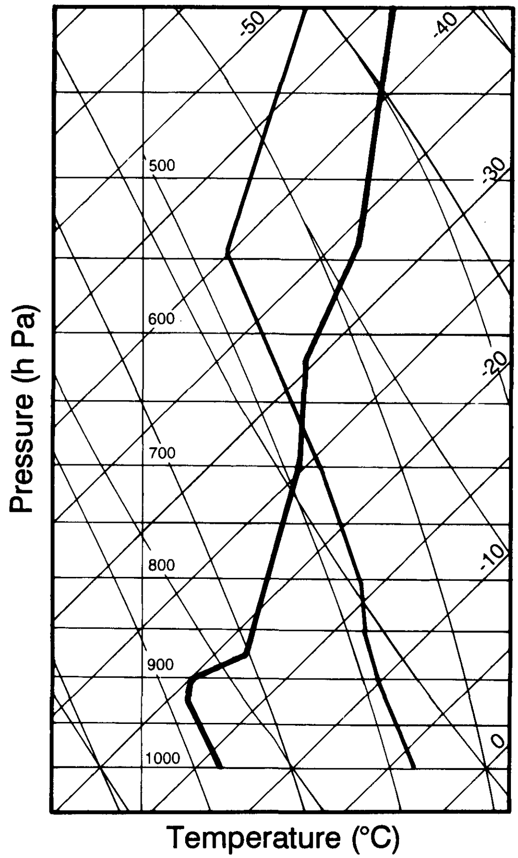

Fig. 6. Temperature soundings from Bear Island at 00 UTC 26 March (thick), 27 March (thin), 1992.

directions, and the measurements in this open sea area are too few to produce detailed surface maps. It is difficult on the basis of these data sources to reveal the exact structure of the system or the relative strength of the individual disturbances. The 1000 hPa windfields calculated by the mesoscale operational model of DNMI at 12 UTC the 24th and the 25th are shown in Fig. 7a, b. The model does not resolve the initial polar low very well and probably mixes the polar low coming in from the west and the vortex advected down from the north (disturbance 2). However, the data support the development described above, indicating a third disturbance further east. Whether the second or the third disturbances are responsible for the intensifying cluster of clouds moving northwards, merging in the afternoon of the 25th, is difficult to determine. The subsequent section

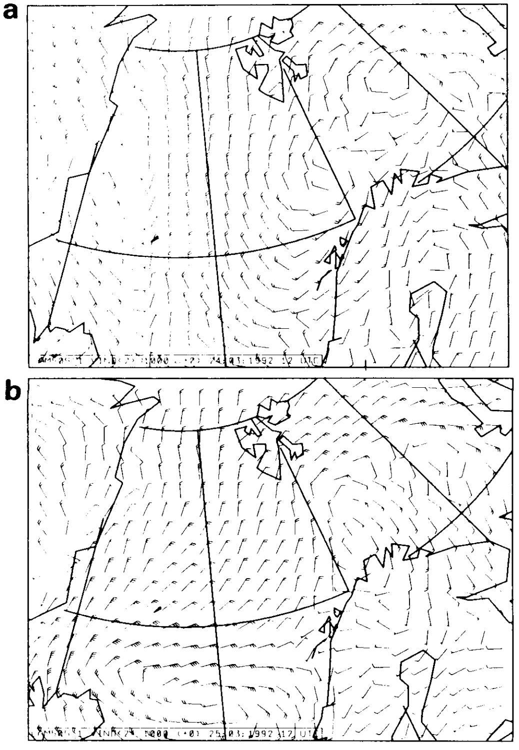

Fig. 7. LAM50 model analysis surface wind at 12 UTC 24 March (a), 12 UTC 25 March (b), 1992, DNMI, Oslo.

will discuss additional information provided by the infrasonic DOA-spectra.

3. Infrasonic signatures

Referring to the map of Fig. 2, the two PBIS stations in northern Norway and at Svalbard are situated close to the extensive regions of the Norwegian, Greenland and Barents Sea area, and may provide a good baseline for triangulation. Depending on the local level of noise (local windspeed), it is expected that these two stations should be able to detect infrasonic signals propagating from distant weather systems more than 1000 km away, due to the very low atmospheric attenuation at these low frequencies.

The PBIS's estimate the directionality of the local background atmospheric noise at the infrasonic frequency range of about 0.2–13 Hz. This noise environment is a mixture of signals produced by different weather phenomena, as well as auroral activity, ocean waves, strong upper atmospheric jets and industrial low frequency noise sources, all covered in local, isotropic turbulence noise depending on the strength of the local winds. Direction-of-Arrival-(DOA)-spectra are evaluated, consisting of individual $32 \times 36 \times 9$ DOA-matrixes, each one containing the number of all signals received within one hour, distributed on 32 frequency components, 36 azimuth sectors and 9 elevation sectors (phase velocity sectors). One DOA-matrix thus represents the one hour averaged directionality of the background atmospheric noise at these frequencies. The term DOA-spectra will hereafter be used for this statistical quantity. Provided that the local turbulence noise is not too strong, the DOA-spectra will output the average directions of distant infrasonic noise generators.

Figs. 8 and 9 show the infrasound plots from both stations in the period 23–27 March. The DOA-spectra are averaged at the selected broad frequency range of 1–12 Hz. The azimuth direction (360° horizon) is folded out along the ordinate, marked by geographical directions W-S- E-N. The time is given in UTC along the vertical axis. The dominating directions of active noise generators turn up in the third dimension by shades of grey, indicating by the number of received signals (see top of plots) in each hour. The right half of the plots show the distribution of the same number of signals for the same frequency range (1–12 Hz). The plot on the far right gives the approximate level of the local windspeed. On all plots as the local wind increases, the DOA-spectra get smeared out, due to a reduced signal-to-noise ratio (SNR), caused by the increased local atmospheric turbulence noise level. Because the intensity of the turbulent pressure perturbations follow a $-7/3$ power law with respect to frequency, the lowest frequencies are generally expected to be the most noisy ones. On the other hand, the highest frequencies will be the weakest signals received from a generator far away, since the attenuation of acoustical waves in the atmosphere is proportional to the square of the wave frequency. More local industrial noise sources are also likely to contaminate the recordings at the highest frequencies, but expected to be narrowband in nature. However, since the variance of the PBIS DOA-estimation increases linearly with decreasing

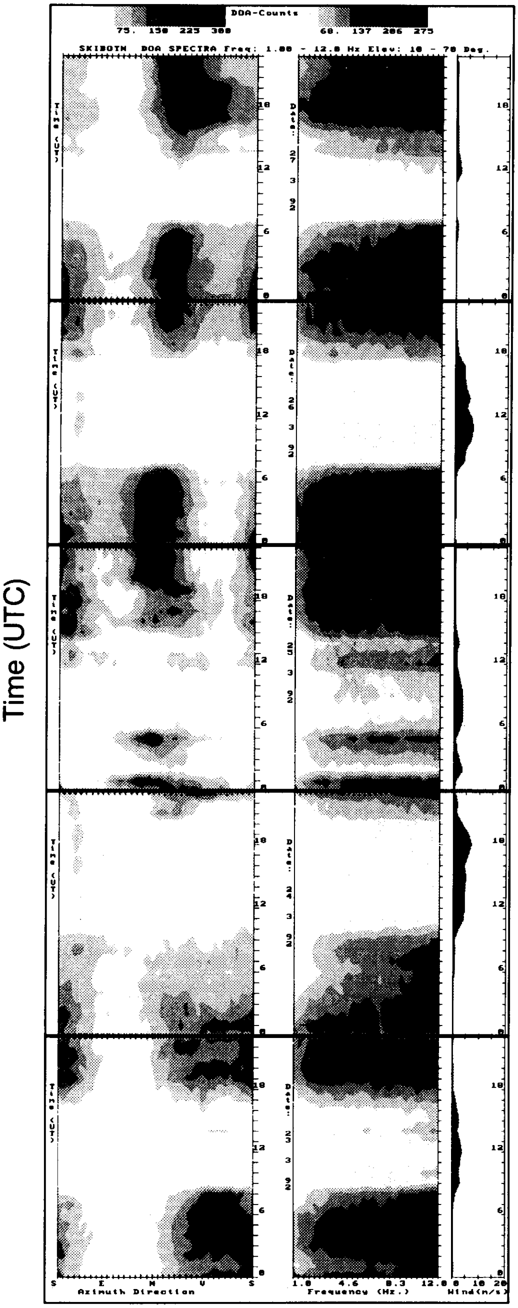

Fig. 8. Skibotn DOA-spectra 23–27 March, 1992, at frequency range 1–12 Hz.

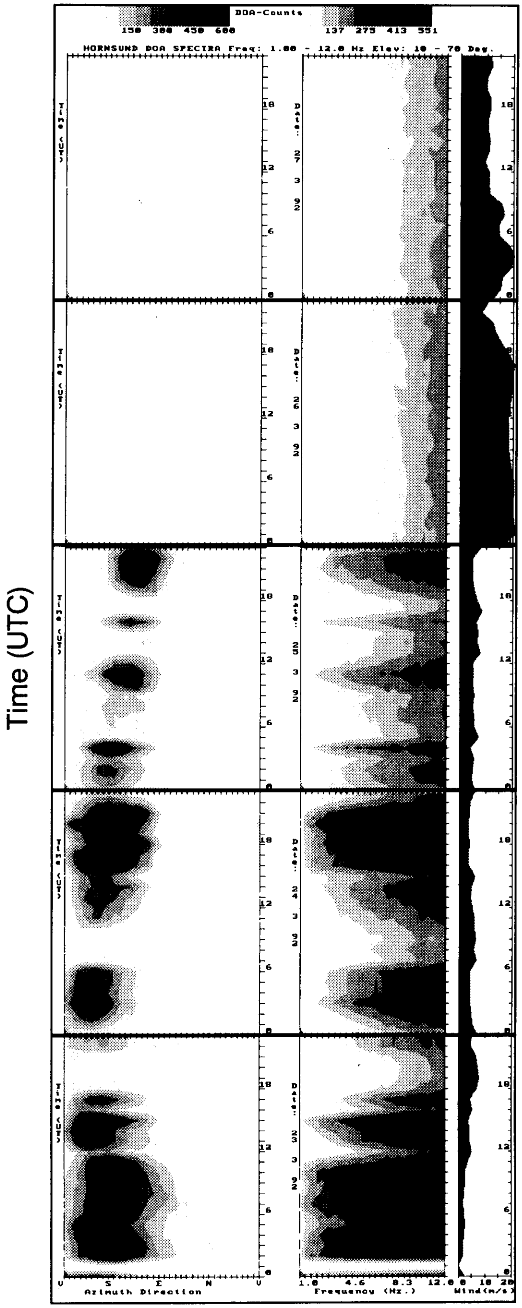

Fig. 9. Hornsund DOA-spectra 23–27 March, 1992, at frequency range 1–12 Hz.

frequency (doubled for each octave downwards), for the same SNR, the system performs best on the highest frequencies (design frequency of the array). It should also be emphasized that the amplitude of the DOA-spectra, i.e., the number of counts, does not critically depend on the strength of the signals received or the strength of the acoustical generators. The amplitudes depend on the SNR, which to a major extent is controlled by the local windspeed level. Lower local winds usually decrease the spread of the received signals.

The DOA-spectra give us the following general information. The Skibotn spectra of Fig. 8 detected infrasonic noise from the southwest (SW) during the 23rd, and in the morning of the 24th, a peak was seen a little south of west, with indication of a diffuse infrasonic generator towards NW. In fact, the weak signals from NW were recorded already on the late evening of the 23rd. During the day, the local wind causes the DOA-spectra to be smeared out, but late in the evening weak signals arrive from the NW, more northwards than in the morning. The next day (25th) the signals come prevailingly from a northerly direction, about 10–30° east of N. The two morning peaks are quite sharp, whereas stronger and broader signals are seen towards night. During the next two days the local wind situation is good at night time, and the DOA-spectra indicate a strong, steady, infrasonic source in the north, moving slowly back westwards from 26 to 27 March. At evening the 27th, the source fills a broad ($\sim 50°$) azimuth sector towards NW–W. Due to a data gap, no signals are received at 08–12 UTC. Some signals are also received from SSE in the period, and at times of local calm wind, the signals show a broadband nature.

On the Hornsund spectra (Fig. 9), signals are seen coming from south and SW during the period of breezy weather up till the evening of the 23rd. The data starts from SW in the morning of the 24th, intensifying at evening towards S. Two extra peaks are seen towards SE. The dynamics of the signals detected during the 25th is very characteristic, with a marked progress slowly from south towards SE during the day. However, the signals are received intermittently. If the same infrasonic generator produced these signals, it should move from a southerly direction with respect to Hornsund in the morning, towards east or NE during the day. Around midnight 25–26 March, the wind increases abruptly to 44 Kn at the station, and the data from the Hornsund PBIS is from now on dominated by the intense turbulence produced by the local wind.

It seems that the Hornsund and Skibotn PBIS's monitor the polar low from its start in the morning of the 24th just west of Skibotn, following its path northeastwards, passing west of Bear Island. The Skibotn DOA-spectra then follow the low on the return between the southern tip of Spitsbergen and Bear Island, and down towards Lofoten, where it makes landfall during the 28th. However, the development during the evening of the 24th and towards midday on the 25th is more structured. As mentioned before, the initial polar low probably reached its highest intensity at approximately 14 UTC on the 24th, and seems to have released its energy during the night 24–25 March. A closer look on the DOA-spectra from the two stations, indicates that several systems interact.

The detailed development occurred during three periods; The development phase during the 24th, the second intensification phase from evening on the 24th throughout the 25th, and the return phase 26–27 March, are described. More detailed DOA-spectra are plotted in Figs. 10 and 11, the Skibotn data at a frequency range of 2–8 Hz, and the Hornsund data at selected frequencies 2–7 Hz. The Hornsund DOA-spectra cover the days 23–25 March (no data received later), whereas the Skibotn spectra cover the last two phases 25–27 March. Referring to the Hornsund DOA-spectra in the morning of the 24th (Fig. 10), signals are seen in the SW quadrant, indicating slight translation to the south towards midday (marked out by a thin line). This signature corresponds to the geographically west towards east movement of the diffuse, intensifying cloud-cluster SW of Svalbard. Later, two strong generators are seen, one in the south and one towards SE, each alternatly being the stronger one during the evening hours. In the morning of the 25th, the southern system is dominant, but with the eastern generator still present (see 08 UTC). Referring to the corresponding satellite image (Fig. 3d), these signatures come from the directions where the second and third disturbances are seen to intensify. By the end of the day, one broad, strong peak is seen SE, corresponding to the intense cloud-cluster of Fig. 5d. The Skibotn spectra of Fig. 11 show two strong peaks towards NE in the morning of the 25th, at

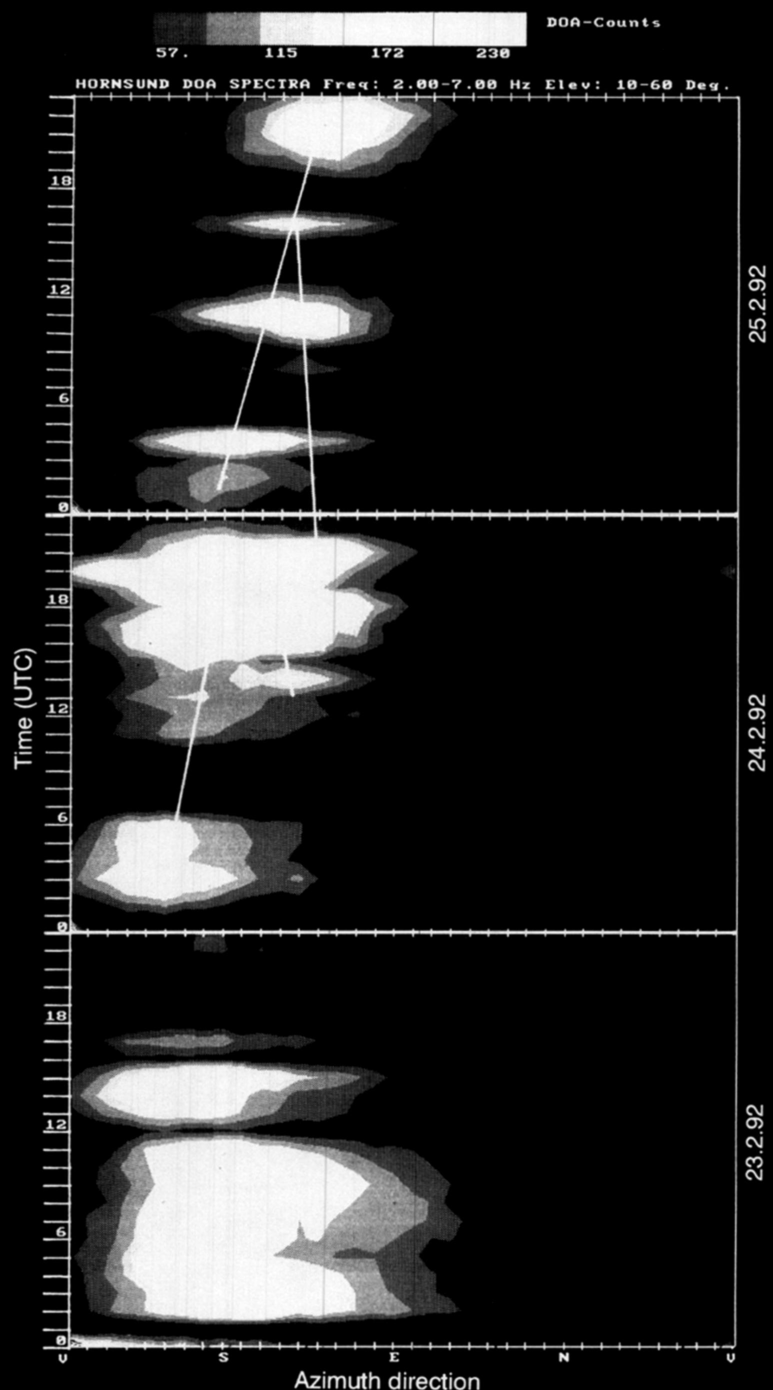

Fig. 10. Hornsund DOA-spectra 23–25 March 1992, at frequency range 2–7 Hz.

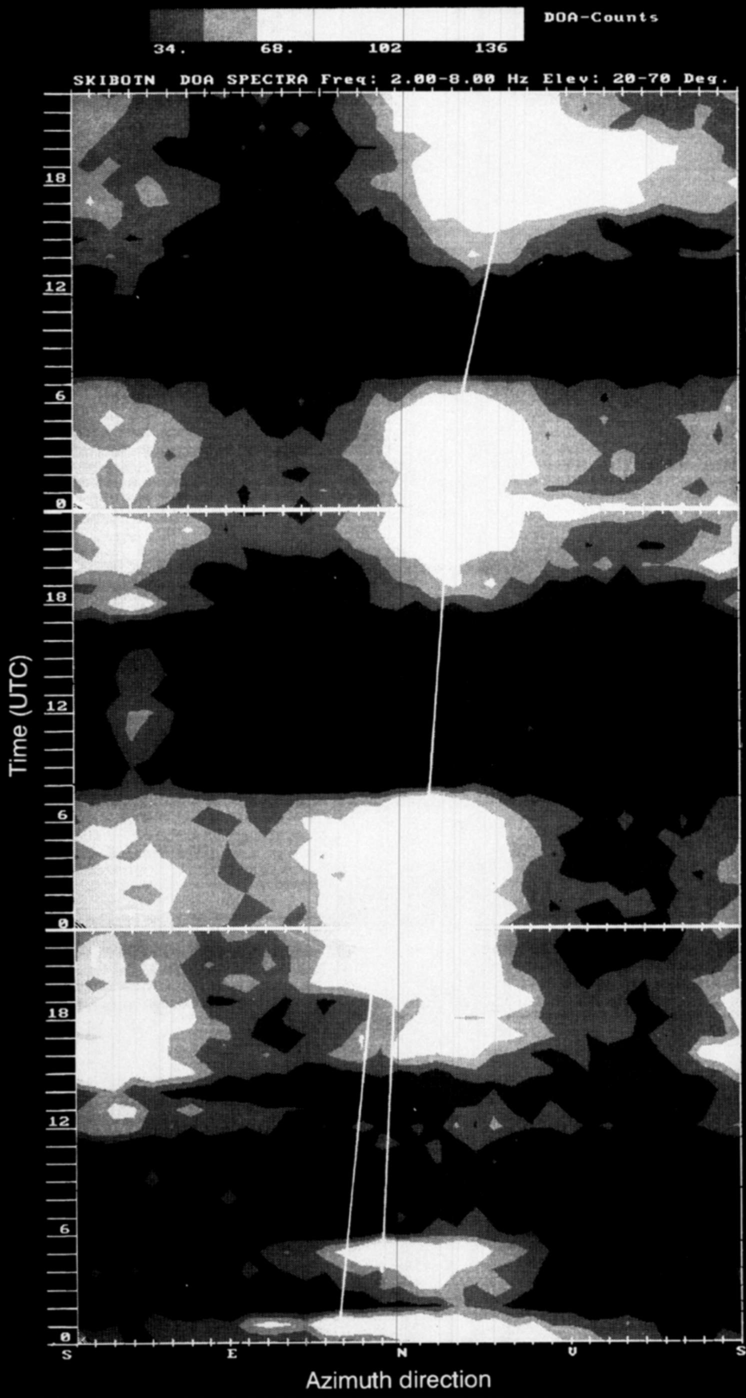

Fig. 11. Skibotn DOA-spectra 25–27 March 1992, at frequency range 2–8 Hz.

1–2 and 5–6 UTC. The signals starting about 30° east of N in the morning move slowly towards N, about 20° during the day. The other peak, starting 10° east of north moves correspondingly westward, and both systems are seen straight north in the evening. It is the authors opinion that these DOA-signatures from the Skibotn and Hornsund stations, are caused by the same two distant generators moving northwards, merging NE of Bear Island in the evening of the 25th.

The complex development can then be summarized as follows; The initial, beautiful polar low vortex seen on Fig. 3c, most probably released its energy during the evening of the 24th. It is detected by the Skibotn and Hornsund PBIS's, moving from west towards north with respect to Skibotn, and SE towards south with respect to Hornsund. The vortex that was advected southwards from Svalbard, preceding the polar low and recognized as the bright convective spot further northeast (disturbance 2), takes over and starts moving northeastwards as the first low remains nearly stationary outside the coast of Finmark. A third disturbance, also developing from a similar vortex further east, moves northwestwards towards the southern tip of Svalbard, revealing its existence by the Hornsund DOA-spectra during the evening of the 24th, as well as by the strong signals seen in Skibotn towards the NE on the morning of the 25th. The satellite images show that the systems grow while moving northwards, developing new convective clouds further and further poleward. The Hopen station reports a 45 Ktn wind at 12 UTC on the 25th, and during the next 12 h the complex system transforms rapidly as the cloud cluster increases in size and blows over the southern tip of Svalbard. This development may have been initiated as the two disturbances merged south of Hopen around 12 UTC, concentrating all the cyclonic vorticity available into maximum intensity between Bear Island and Spitsbergen. The broad PBIS data at Skibotn then tracks the mature low back again during the days 26–27 March, until it passes Lofoten on its way southwards.

4. Discussion and conclusions

The case study presented in this article reveals that the polar low development actually consists of three interacting disturbances, each one having separate origins. The second and the third disturbances are seen on the satellite images as small, shallow vortices, generated along the secondary baroclinic zones set up where the sea surface temperature show large gradients; along the western coast of Svalbard down to Bear Island, and NE of northern Norway, where the Golf stream ends its path into the Barents Sea. The first disturbance has its origin in the area between Jan Mayen and Greenland. All three systems intensify during the 24th, at the time upper level positive vorticity is advected into the area.

To summarize, the set of meteorological and infrasonic observations are put together in Fig. 12, where the directions of peak intensity of the received signals at both Hornsund and Skibotn stations are plotted down at selected times together with the cloud-cluster positions. The only criterion for selecting the direction of an infrasound generator, is that there is a local maximum in the DOA-spectra, picked out manually from Figs. 10 and 11. The most intense clouds are drawn "by hand" from the corresponding satellite images (but the reader should compare the respective images in either case). The size of the marked sectors are the selected 10° azimuth resolution of the DOA-spectra. The plots strongly suggest that the DOA-spectra follow the movements of the active cloud systems. The Hornsund station monitors the initial polar low in the south from its very start as a diffuse cloud-cluster (Fig. 12, 1), as well as through its intensive phase in Fig. 12, 2–3. The same figures also show that the Hornsund station detects the second and third disturbances towards SE during the 24th. During the morning of the 25th, signals seem to be generated from the western part of the cloud-cluster drifting northwards (Fig. 12, 4–6). However, from about 08 UTC, the signals are received from SE, more and more eastwards during the day (Fig. 12, 6–8). In Fig. 12, 8 the directions of arrival for the whole evening are marked simultaneously, the earliest received signals being the most southward. From the evening of the 25th until evening of the 27th (Fig. 12, 8–12), the Skibotn DOA-spectra follow the movements of the low, with signals received first slightly east of north, rotating westward and ending up SW by the end of the 27th. During the 27th, the long, convective front zone seen on the satellite pictures seem to produce more infrasound

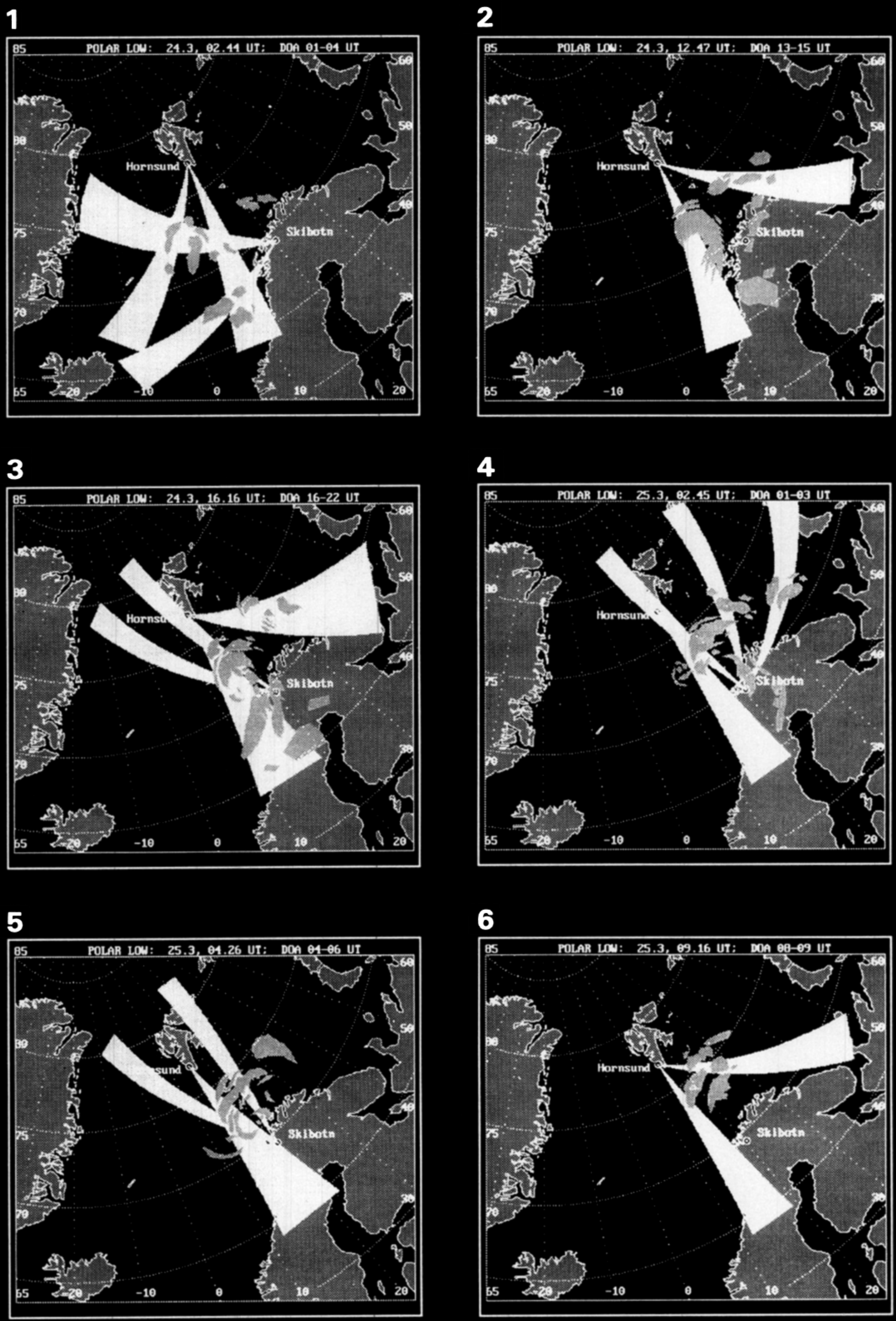

Fig. 12. DOA-Cloud-cluster plots at 12 different UTCs, 24–27 March, 1992.

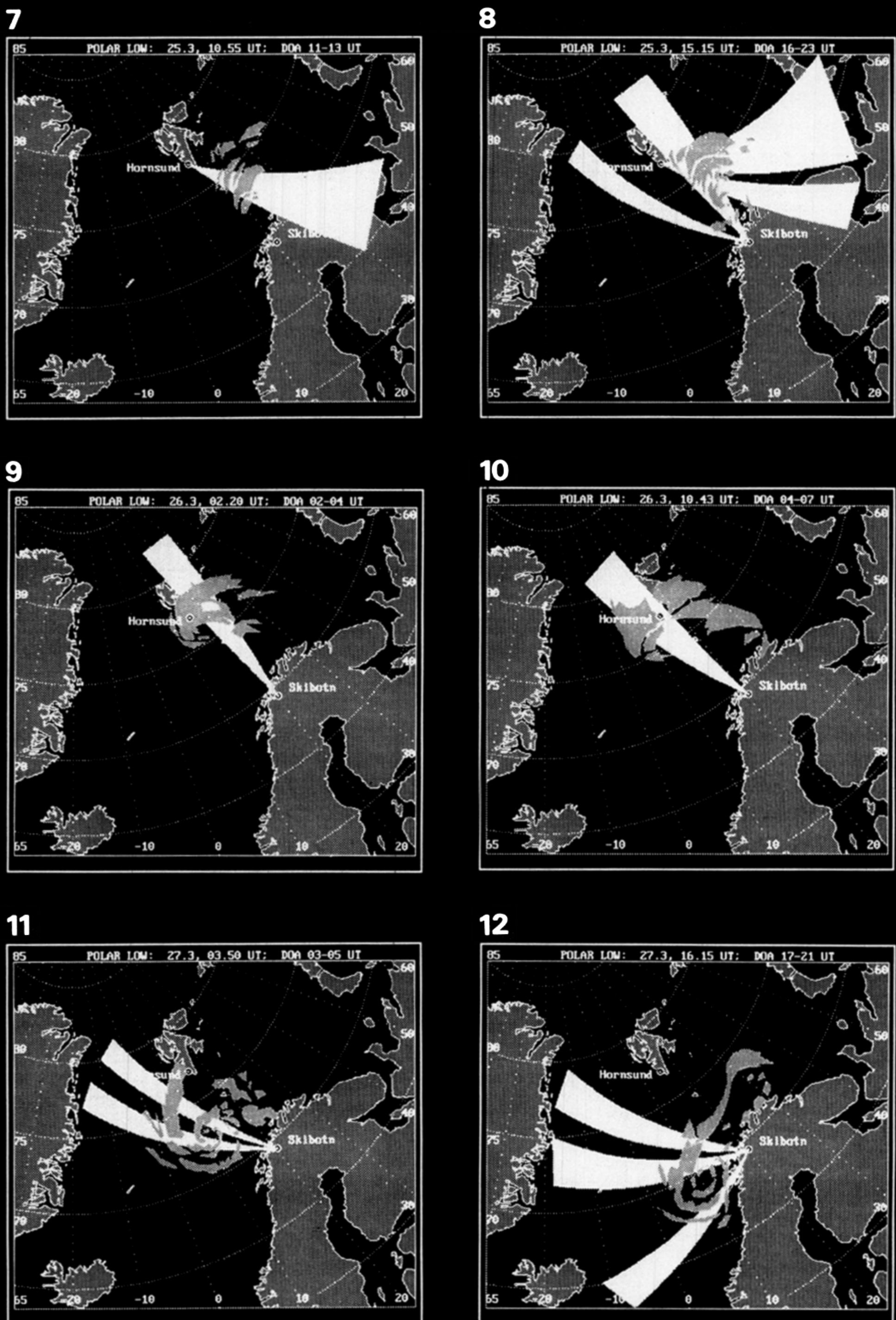
7
POLAR LOW: 25.3, 10.55 UT: DOA 11-13 UT
Hornsund
8
POLAR LOW: 25.3, 15.15 UT: DOA 16-23 UT
Skibotn
9
POLAR LOW: 26.3, 02.20 UT: DOA 02-04 UT
Skibotn
10
POLAR LOW: 26.3, 10.43 UT: DOA 04-07 UT
Skibotn
11
POLAR LOW: 27.3, 03.50 UT: DOA 03-05 UT
Skibotn
12
POLAR LOW: 27.3, 16.15 UT: DOA 17-21 UT
Hornsund
Skibotn

Fig. 12 (cont'd).

than the low centred more to the south. Returning to the morning of the 24th, the Skibotn data also detect the early diffuse cloud cluster towards NW, but the local windfield in Skibotn behind the polar low caused high local levels of noise during the day, and the DOA-spectra are smeared out. The northeastern signals in Fig. 12, 3–4, are interpreted as being generated by the second and third disturbances moving northwards. Closer disturbances like the rest of the first polar low, remaining nearly stationary off the coast, may also be potential infrasonic generators, but the disturbances moving northwards are the most likely sources, being the active, developing parts of the weather system.

Because the local wind at the Hornsund station was very stable at about 8 m/s the whole day of the 25th, the intermittent reception of signals could be due to a propagation effect, or reflect dynamical processes in the acoustic generator. The DOA-spectra (Fig. 10) show broad, independent peaks, intensifying and fading away, each new one more eastwards than the other. This is also what is seen in the satellite pictures (Fig. 5a–d). The new convective clouds taking part in the development, bubble up in a position northward of the preceding one, or more eastward as seen from Hornsund. The authors believe that this is what causes the intermittent signals at the Hornsund station; the dynamic development of the cloud cluster, with the new active clouds turning up on the northern side of the disturbance area. The Skibotn data also show a rather discrete nature during the 24th and the 25th, but from the time the development ended up as a mature low with extensive clouds covering a large part of the Svalbard area, the Skibotn spectra are significantly broader.

One additional detail in this respect is worth mentioning. Fig. 12, 1 shows that the Skibotn station receives signals also from SW in the morning of the 24th (and evening of the 23rd), indicating that the bright clouds seen in the same direction south of Lofoten (Fig. 3b) are active. The cloud-cluster moves quickly on shore before 12 UTC (cf. Fig. 3c), but after this time, no signatures of the visible cloud-cluster can be seen in the DOA-spectra (cf. Fig. 8 and Fig. 12, 2–3). A closer examination of the surface maps shows that the wind direction at Bodø indicates a disturbance entering the coast south of the station around 12 UTC, and the windspeed jumps up from 10 to 30 Kn for a couple of hours. Obviously, the diffuse cloud-cluster was a fourth, active disturbance, detected by the Skibotn PBIS. As this fourth little low went on shore, the energy supply from beneath, driving the convective currents, was turned off, and the disturbance rapidly decayed. Although the clouds are seen just as bright on the images, the system was not convective after entering land, and the acoustical noise generator was turned off.

During periods of low local wind, signals are often seen in Hornsund from the SW. For example, a closer analysis of the Hornsund DOA-spectra of the 23rd (Fig. 9), reveals that the strong signals from SW seen at about 4 and 14 UTC, are mainly high frequency signals, whereas the signals from south seen at 2, 6 and 10 UTC are found strongest at medium frequencies. The Skibotn station also receives noise regularly from SSE, especially low frequency signals. The origin of these signals and the principal source mechanism for the presented infrasonic signatures, are not discussed in the present work, but it is clear that turbulent convection may not be the only possible generation mechanism. Ocean waves (Benioff and Gutenberg, 1939) and mountain associated waves (Rind and Donn, 1978) have also been reported in the literature as infrasonic generators, and there may also exist other infrasonic source mechanisms more directly connected to the shear layers or the vortical flowfields (Lighthill, 1952), as well as the pressure perturbations produced directly from the release of latent heat. The secondary baroclinic zone along the western coast of Svalbard down to Bear Island should in this respect be studied more carefully, as vorticity continuously is generated along this zone. The turbulent boundary layer fluxes of moisture and heat are also especially strong during the periods of polar air outbreaks, producing stratocumulus streets reaching the low level inversion at 1–2 km heights. The acoustic emission from these clouds should be very weak, although they cover practically all of the Norwegian- and Barents-Sea region. It is also clear that the multitude of waves in the ocean region of interest may be a continuous source of infrasound.

A closer look into the DOA-matrixes is necessary to get more detailed information and separate individual signals from different sources and at different frequency, azimuth and phase speed. However, the simple technique used here prevents any separation of signals from for example turbulent convection and ocean waves, which neighter is attempted, although the strongest wind fields and consequently the worst sea is normally found SW of the polar low cyclone centre (PLP, 1986), giving a possible method of separation. The present discussion restricts itself to those infrasonic signatures that can be correlated to dynamical features of the cloud patterns. Referring to the model wind data of Fig. 7b and the corresponding DOA-spectra of the 25th (Fig. 11), a strong synoptic scale cyclone is seen passing the Norwegian-Sea from Iceland to southern Norway, but no infrasound is detected from the system. The winds and shear layers are stronger for the synoptic low, but the clouds are lower (as seen from the satellite images), and the vertical velocities along the fronts are also expected to be lower than compared to the polar low case.

It seems reasonable to suggest that the convective processes are probably the strongest acoustic noise source in this case. It is the convective nature of these polar instability lows that especially divides them from their synoptic big brothers. The CISK mechanism describes how the individual convection cells interact with the cyclonic disturbance on the scale of the polar low, having dimensions 2 orders of magnitude larger (3–400 km), and with deep and vigorous convection primarily confined to the centre of the polar lows. This ideal situation may, however, not actually occur. By detecting the most intense, convective parts of the lows, the infrasonic DOA-spectra should be able to separate individual disturbances, as well as monitor the temporal variations of convective processes involved. Further study of infrasound generated from these instability lows, also involving the frequency content of the signals, together with measurements of cloud top temperature, giving a measure of the convective intensity of the clouds, may therefore give more insight to the dynamical and geographical fine structure of the phenomena, as well as a closer approach to the generation mechanism.

Thus, strongly supported by the plots of Fig. 12, it is concluded that polar lows apparently generate strong infrasound, and it is suggested that the emitted signals most probably are produced in the regions of intense, convective clouds of the developing low. The signals are remotely detected by the Hornsund and Skibotn PBIS-stations 500–1000 km away, and the presented infrasonic DOA-spectra show that the two stations were able to monitor the polar low from its initial start as a diffusive cloud-cluster, along the track of new intensification, until it made landfall 4 days later. The infrasound data also clearly show that several disturbances were present in the complex development.

It is tempting to suggest future continuous measurements from a distributed set of PBIS stations around the ocean area of interest, in order to get a more statistical database for the studies. Under the assumption that the PBIS systems are able to detect the areas of vigorous convection, the technique may serve as an additional data source to the conventional observations, and provide corrective inputs to the numerical prediction models, in much the same way as the satellite images are used. However, although the satellite images are important for detecting the initial vortices, they are always ambiguous with respect to the state of the clouds and do not give information about the dynamics of the disturbances, other than by comparing subsequent images. Given the above hypothesis, the DOA-spectra may on the contrary tell us if the cluster of clouds is convective, i.e., if the system is still active and developing, giving an immediate view of the dynamics, delayed by the propagation time of infrasound. The active, convective parts of the system, or new intensification of these, are monitored in near real time. As for the practical and operational capabilities of this passive acoustic remote sensing technique, this is significantly limited by the high sensitivity to local wind noise. The DOA-spectra are smeared out when high local winds significantly increase the variance of the received signals. The local calm periods therefore act as windows to the world outside, giving short "glimpses" of the possible infrasonic generators present around the 360° horizon. A distributed set of PBIS stations should have a better probability of giving continuous data output.

5. Acknowledgments

This article is written as part of a Dr. Scient. Study financed by the Royal Norwegian Council for Scientific and Industrial Research. Financial aid concerning the field work is also given from the

Norwegian Polar Research Institute and "Nansenfondet". Thanks also to The Department of Physics for financial help during the last 5 months.

Specially warm thanks is given to my supervisor Professor Alv Egeland for his never absent incentives! Many thanks is also given to Åsmund Rabbe for important discussions concerning Polar Low events. Thanks also to Magne Lystad at The Norwegian Meteorological Institute for providing the model analysis wind-data included in the report.

The PBIS system in Hornsund has been able to withstand the hard arctic climate thanks to the staff at The Polish Research Station there. The measurements would have been totally impossible without the great help from them. The Skibotn PBIS station has been looked after by Professor Ove Harang, Univ. of Tromsø, Norway.

REFERENCES

Benioff, H. and Gutenberg, B. 1939. Waves and currents recorded by electromagnetic barographs. *Bull. Amer. Meteor. Soc.* **20**, 421–426.

Bowman, H. S. and Bedard, A. J. 1971. Observations of infrasound and subsonic disturbances related to severe weather. *Geophys. J. R. Astr. Soc.* **26**, 215–242.

Georges, T. M. 1973. Infrasound from Convective Storms: Examining the Evidence. *Rev. Geoph. Space Phys.* **11**, 571–594.

Goldreich, P. and Kumar, P. 1990, Wave generation by turbulent convection. *Astrophys. Journal* **363**, 694–704.

Lighthill, M. J. 1952. On sound generated aerodynamically (I). General theory. *Proc. Roy. Soc. London* **A211**, 564–587.

Liszka, L. 1977. Infrasonic waves-interaction with the atmosphere. In: *Dynamical and chemical coupling* (ed. Grandal and Holtet). Holland: Reidel, pp. 63–71.

PLP. 1986. *Polar lows project-final report, polar lows in the Norwegian, Greenland and Barents Sea* (ed. Lystad). Oslo/Norway: The Norwegian Meteorological Institute.

Rabbe, Å. 1975. Arctic instability lows. *Meteorologiske Annaler* **6**, 303–329.

Rabbe, Å. 1987. A Polar Low over the Norwegian Sea, 29 February–1 March 1984. *Tellus* **39A**, 326–333.

Rasmussen, E. 1985. A case study of a Polar Low development over the Barents Sea. *Tellus* **37A**, 407–418.

Rind, D. H. and Donn, W. L. 1978. Infrasound observations of variability during stratospheric warmings. *J. Atmos. Sci.* **35**, 546–553.

Stein, R. F. 1967. Generation of acoustic and gravity waves by turbulence in an isothermal stratified atmosphere. *Solar Physics* **2**, 385–432.

Økland, H. 1987. Heating by organized convection as a source of Polar Low intensification. *Tellus* **39A**, 397–407.

Økland, H. 1989. On the genesis of Polar Lows. In: *Polar and Arctic Lows* (ed. Twitchell, Rasmussen and Davidson). Deepak Publishing, 179–190.

Ørbæk, J. B. 1992. Passive broadband infrasonic sodar at the University of Oslo (II). *Department of Physics, Report Series 92–35*, University of Oslo/Norway.